ARTICLE

OBC
www.rsc.org/obc

# Nucleophilic and general acid catalysis at physiological pH by a designed miniature esterase†

**Andrew J. Nicoll and Rudolf K. Allemann***
*School of Chemistry, University of Birmingham, Edgbaston, Birmingham, UK B15 2TT.*
*E-mail: r.k.allemann@bham.ac.uk; Fax: +44-1214147871; Tel: +44-1214144359*

***Received 30th March 2004, Accepted 14th June 2004***
***First published as an Advance Article on the web 8th July 2004***

A 31-residue peptide (Art-Est) was designed to catalyse the hydrolysis of *p*-nitrophenyl esters through histidine catalysis on the solvent exposed face of the α-helix of bovine pancreatic polypeptide. NMR spectroscopy indicated that Art-Est adopted a stable 3-dimensional structure in solution. Art-Est was an efficient catalyst with second order rate constants of up to 0.050 $M^{-1}$ $s^{-1}$. The activity of Art-Est was a consequence of the increased nucleophilicity of His-22, which had a reduced p$K_a$ value of 5.5 as a consequence of its interaction with His-18 and the positively charged Arg-25 and Arg-26. Mass spectrometry and NMR spectroscopy confirmed that the Art-Est catalysed hydrolysis of *p*-nitrophenyl esters proceeded through an acyl-enzyme intermediate. A solvent kinetic isotope effect of 1.8 indicated that the transition state preceding the acyl intermediate was stabilised through interaction with the protonated side-chain of His-18 and indicated a reaction mechanism similar to that generally observed for natural esterases. The involvement in the reaction of two histidine residues with different p$K_a$ values led to a bell-shaped dependence of the reaction rate on the pH of the solution. The catalytic behaviour of Art-Est indicated that designed miniature enzymes can act in a transparent mechanism based fashion with enzyme-like behaviour through the interplay of several amino acid residues.

## Introduction

Small, unstructured peptides seldom display functional activity. Naturally occurring enzymes and proteins on the other hand typically depend for activity on large and complex folds to hold in place a relatively small number of functionally important residues. The design of small structurally well-defined peptides that serve as alternative scaffolds to hold functional groups in reactive orientations has developed into an active area of research.[1]

We and others have recently described the design of miniature proteins that bind DNA with high affinity.[2–5] In the case of ApaMyoD, where the recognition α-helix of the basic helix–loop–helix–protein was stabilised by disulfide bonds to a N-terminal extension based on the peptide apamin, the DNA binding specificity and affinity could be controlled by the redox state of the miniature protein.[5] Pancreatic polypeptides (PP) have been used as scaffolds for molecular recognition processes based on α-helices to create DNA binding proteins[2–4] and miniature enzymes.[6,7] The introduction of lysine residues into the α-helix of PPs led to the production of Oxaldies-3 and -4, highly efficient miniature enzymes that catalyse imine formation with the substrate oxaloacetate with rate enhancements of almost 4 orders of magnitude relative to catalysis by simple amines such as *n*-butyl amine.[8] These miniature proteins catalysed the reactions with Michaelis–Menten kinetics and in the case of Oxaldie-4, which was based on bovine PP (bPP),[9] displayed relatively high stabilities.[7] The thermal denaturation of Oxaldie-4 showed a sharp unfolding transition with a melting temperature of 50 °C. Considering the small globular shape of Oxaldie-4, the high melting temperature is remarkable and suggested a compact structure. Similarly, Oxaldie-4 displayed high resistance to denaturation with urea.

One of the key issues in the generation of miniature enzymes is whether, in the absence of an active site pocket, they can act in a transparent mechanism based fashion through the interplay between several amino acid residues. In the case of Oxaldie-4, the enhanced reactivity of the miniature enzyme relative to simple amines was based on a preponderance of positively charged amino acid residues on one face of the α-helix, which led to a depression of the p$K_a$ and increased the speed of the formation of the imine intermediate.[7] Here we show the high versatility of scaffolds based on bPP for the generation of miniature enzymes with activities other than β-ketoacid decarboxylases. An artificial esterase (Art-Est) was designed to catalyse the hydrolysis of *p*-nitrophenyl esters at physiological pH (Scheme 1). Its activity is based on a stable 3-dimensional structure in solution and the cooperative behaviour of two histidine residues introduced into the α-helix of bPP. One of the histidines acted as the nucleophile and the other as the general acid catalyst leading to stabilisation of the anionic transition state and a rate enhancement of more than two orders of magnitude relative to catalysis by 4-methylimidazole within the pH window where the $HisH^+$–His pair was in the correct protonation state.

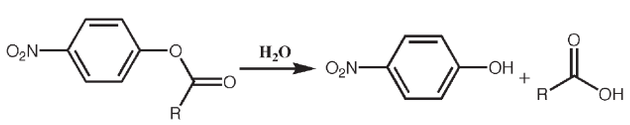


**Scheme 1**

## Experimental

### Materials

All chemicals and biological buffers were purchased from Sigma Aldrich. Mono-*p*-nitrophenyl fumarate was synthesised as described previously.[10] Amino acids and reagents for peptide synthesis were from Novabiochem or Applied Biosystems.

### Peptide synthesis and purification

Art-Est was synthesised using a Pioneer Perceptive Biosystems automated peptide synthesiser and standard Fmoc protocols. The Fmoc and side-chain protected amino acids (Asn, Gln, His (Trt); Asp, Glu ($O^tBu$); Tyr, Thr ($^tBu$) and Arg (Pbf)) were coupled to Fmoc-5-(4-aminomethyl-3,5-dimethoxyphenoxy) valeric acid on a polyethylene glycol support. Prior to cleavage and deprotection with 10 ml 2,2,2-trifluoroacetic acid (TFA) : water : phenol : tri-isopropylsilane (88 : 5 : 5 : 2; v/v) per gram of resin for two hours at room temperature, Art-Est was acetylated with acetic anhydride (0.5 M), diisopropylethylamine (125 mM), *N*-hydroxybenzotriazole

† Electronic supplementary information (ESI) available: NOESY and TOCSY spectra; Table with NMR assignments and observed NOEs; complete set of kinetic data for Art-Est catalysis; mass spectrum of fumaryl-Art-Est intermediate; rate constants for the spontaneous and catalysed ester hydrolysis. See http://www.rsc.org/suppdata/ob/b4/b404730c/. Coordinates for the structure of Art-Est have been deposited in the Brookhaven Protein Data Bank, code 1v1d.

DOI: 10.1039/b404730c

(15 mM) in *N*-methyl-pyrrolidone using 2-(1*H*-benzotriazole-1-yl)-1,3,3,3-tetramethyluronium hexafluorophosphate for activation. The resin was removed by filtration and the soluble products concentrated *in vacuo* and precipitated by washing with 3 × 5 ml of ice-cold diethyl ether. The peptide was disolved in 50 ml of 10% acetic acid followed by lyophilisation. The peptide was redisolved in 10 ml 0.05% TFA and purified by reversed-phase HPLC on a LUNA 10 μ $C_{18}$ column (250 × 21.2 mm). The peptide was eluted with a linear gradient from 23.4–30.6% acetonitrile in water (0.05% TFA) with a flow rate of 5 ml $min^{-1}$ over 60 min followed by a 20 min isocratic run at 30.6% acetonitrile during which time Art-Est eluted. Solvent was removed *in vacuo* followed by lyophylisation. Art-Est was identified by MALDI-TOF and ESI-TOF mass spectrometry. The experimentally determined masses were 3724.3 and 3725.4, respectively, which agreed well with the calculated mass of 3725.3. The purity of Art-Est was shown to be greater than 98% by HPLC on an analytical LUNA 10 μ $C_{18}$ column (250 × 4.6 mm).

### NMR spectroscopy

NMR spectra were recorded using a 6.0 mM sample of Art-Est $H_2O$ : $D_2O$ (90 : 10) at pH 5.4. $^1H$–$^1H$ TOCSY and NOESY spectra were recorded using standard pulse sequences and WATERGATE solvent suppression, running on a Bruker Advance 500 MHz spectrometer. The TOCSY was acquired with 58 ms DIPSI-2 spin lock in a 10 kHz $B_1$ field, and processed with a sine-bell window function, shifted by π/2. The NOESY was acquired with a 200 ms mixing time and processed with a sine-bell window function, shifted by π/2. The resonances were assigned using standard NMR procedures.[11] A set of distance constraints were derived from a NOESY spectrum recorded with a mixing time of 200 ms and integrated according to the cross-peak strengths. The distance constraints were classified into four categories corresponding to inter-proton distance constraints of 1.8–2.8, 1.8–3.5, 1.8–4.75, and 1.8–6.0 Å. Hydrogen bond constraints were imposed on a number of protein backbone NH groups which were observed to form standard α-helical hydrogen bonds. For hydrogen bond partners, two distance constraints were used where the distance (D)H–O(A) corresponded to 1.5–2.5 Å and (D)N–O(A) to 2.5–3.5 Å. Structures were calculated from an extended conformation using CNS.[12] A standard simulated annealing protocol containing torsion angle dynamics was used to create 20 structures where no distance violation in the protein structure was larger than 0.3 Å and no angle violation was greater than 5 degrees.

The NMR titrations for the determination of the p$K_a$ values of the histidines in Art-Est were performed at 290 K using 6.0 mM Art-Est in $D_2O$ on a Bruker AC 300 MHz spectrometer. The chemical shifts of the H2 and H4 protons of the imidazole rings of His-18 and His-22 were measured as a function of pH* (uncorrected) with the assumption that the isotope effects cancel out.[13] The two titration curves were clearly resolved and assigned to histidines from the chemical shifts at pH* 5.4. The p$K_a$ values were determined from the titration curves by fitting curves describing the titration of a mono-protonic acid. The pH* of the solution was adjusted through the addition of 100 mM NaOD.

The NMR analysis of the time course of the hydrolysis of mono-*p*-nitrophenyl fumarate was performed at 25 °C on a Bruker Advance 500 MHz spectrometer. 0.5 ml of Art-Est (3.75 mM) was dissolved in potassium phosphate buffered $D_2O$ (50 mM). 0.25 ml of buffer saturated with mono-*p*-nitrophenyl fumarate was added to the peptide solution to give a reaction mixture with a final peptide concentration of 2.5 mM, an initial substrate concentration of 6.6 mM and a pH* of 6.0. The initial substrate concentration was determined by adding 10 μl of the reaction to 500 μl of 0.1 M NaOH. The concentration of the resulting solution of *p*-nitrophenolate was determined from its absorption at 400 nm and an extinction coefficient $\varepsilon_{400}$ of 18000.

### Circular dichroism spectroscopy

CD experiments were performed using a Jasco J-810 spectropolarimeter in 1, 5, or 10 mm cells. Thermal denaturation experiments were carried out with 20 μM Art-Est between 2–82 °C. The temperature gradient used was 0.5 °C $min^{-1}$ for all CD experiments. All samples were dissolved in 5 mM potassium phosphate buffer (pH 7.0) and equilibrated overnight before analysis. pH experiments were performed with 30 μM Art-Est in 5 mM sodium acetate (below pH 5) or potassium phosphate (above pH 6).

### Kinetic parameters

Kinetic runs were carried out on a Shimadzu UV-2101PC spectrometer equipped with a Shimadzu CPS thermocontroller in 100 mM buffer (sodium acetate was used for experiments at pH < 5.1, MES for pH values between 5.6 and 6.6, and MOPS for the pH range 7.1–8.1) at 290 K. The production of *p*-nitrophenol was monitored at 320 nm. The pseudo-first order rate constants were determined in the presence of excess peptide (180–450 μM). Due to the low solubility of the substrates in aqueous buffers, substrates were dissolved in acetonitrile to give substrate stocks of 7.4 mM. 7.5 μl of this solution was mixed with 600 μl of temperature equilibrated peptide solution in a semi-micro cuvette of 5 mm path-length to give a final substrate concentration of 91 μM. The concentrations of the peptide were determined by quantitative amino acid analysis. The second order rate constants were determined by linear regression of the experimentally determined pseudo-first order rate constants as a function of the concentration of Art-Est. The reported rate constants are all the average of at least 3 independent measurements that did not differ by more than 5%.

The proton inventory was performed at pH 5.1 with 400 μM peptide and a final substrate concentration of 91 μM, with varying concentrations of $D_2O$. $H_2O$ and $D_2O$ buffers were prepared separately with the standard correction of pH = pD + 0.4.

## Results and discussion

### Design and synthesis of Art-Est

The design of Art-Est (Fig. 1) was based on the sequence of bPP, an anti-parallel helix–loop–helix protein comprising of a N-terminal polyproline type-II helix that is connected to the C-terminal α-helix by a type II β-turn.[9] Pancreatic polypeptides form stable dimers over wide ranges of concentration and pH.[14,15] The five C-terminal residues (32–36) of bPP, which do not adopt a well-defined structure in solution and are not thought to contribute to the PP fold,[9] were not included in Art-Est. Two histidine residues replaced Ala-18 and Ala-22, residues located on the solvent exposed face of the α-helix of bPP. The close proximity of these histidines suggested a reduced p$K_a$-value due to the unfavourable electrostatic interaction of two protonated imidazoles. His-22 was anticipated to act as the reactive nucleophile due to its proximity to two arginine residues in $i$ + 3 and $i$ + 4 positions, namely Arg-25 and Arg-26. Glu-23 in bPP was replaced by glutamine so as not to counteract the effect of the positively charged residues located around His-22 through the formation of a stabilising interaction with $ImH^+$ of His-22. The two guanidinium groups of Arg-25 and Arg-26 might also help bind the carboxylate group of the substrate, mono-*p*-nitrophenyl fumarate.

The p$K_a$ value of His-18 was expected to be higher than that of His-22 due to the absence of positively charged residues in its vicinity (Fig. 1). In addition, the negatively charged side-chain of Glu-15 was only one helical turn away, allowing the formation of a salt bridge and stabilising the protonated form of His-18. $ImH^+$ of His-18 should therefore help polarise the ester group, thereby facilitating attack of the carbonyl by His-22. $HisH^+$-18 could stabilise the tetrahedral intermediate formed during hydrolysis. The pre-organisation of these residues on the surface of Art-Est was expected to produce a well-defined active site capable of catalysis under physiological conditions in the relatively narrow pH window where, in its deprotonated form, His-22 could act as the nucleophile of the reaction while the protonated imidazole ring of His-18 could help stabilise the anionic transition state. At lower pH values, protonation of His-22 should prevent the reaction, while at high values of pH the rate of the reaction was expected to decrease due to the deprotonation of His-18.

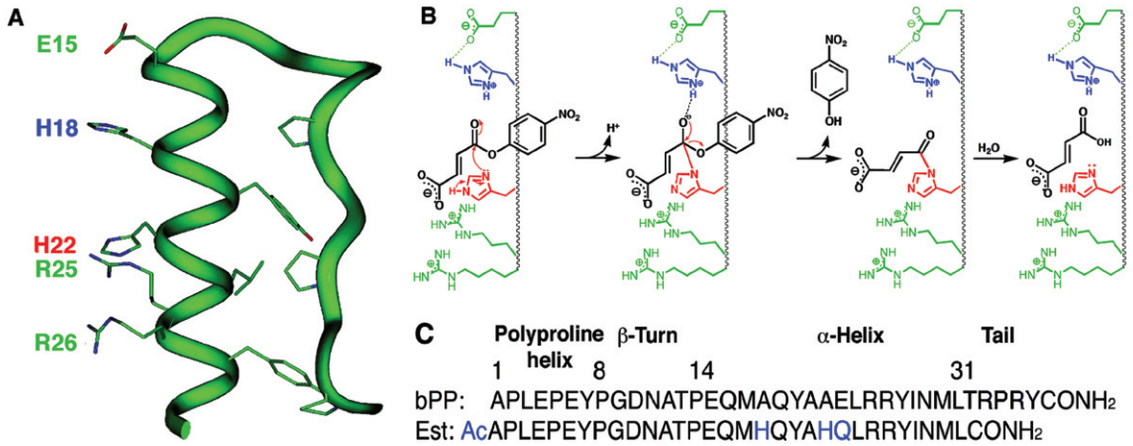


**Fig. 1** A, Representation of the design of Art-Est based on its solution structure as determined in this study. The catalytically important residues are highlighted. B, Proposed mechanism of the Art-Est catalysed hydrolysis of mono-*p*-nitrophenyl fumarate through the interplay of several amino acid residues on the solvent exposed face of the α-helix of Art-Est. C, Sequence alignment of bPP and Art-Est. Residues altered to generate a catalytically active peptide are in blue.

Art-Est was synthesised by solid-phase peptide synthesis using standard Fmoc chemistry. The N-terminal amino group was acetylated with acetic acid to prevent its involvement in the reaction.[8] The peptide was purified by C18 reversed phase HPLC to apparent homogeneity. It was identified by MALDI-TOF and electrospray ionisation mass spectrometry. The mass of 3725 observed for Art-Est by ESI-MS was identical to that calculated for the acetylated peptide.

### Structure of Art-Est in solution

The CD spectrum of Art-Est was typical of those observed for α-helical peptides and resembled that of bPP (Fig. 2A). The spectrum displayed minima at 208 nm and 222 nm with mean residue ellipticities, $[\Theta]_R$, of −6284 ± 150 and −8055 ± 230 deg cm$^2$ dmol$^{-1}$ residue$^{-1}$, respectively. The CD spectrum was independent of the concentration of the peptide for the whole concentration range studied (10–200 μM) (Fig. 2A).

The thermal stability of the structure of Art-Est was measured by CD spectroscopy (Fig. 2B). Two isodichroic points at 204 nm and 238 nm, were observed for the thermal melting of Art-Est indicating that the peptide unfolded without the population of an intermediate state. The thermal denaturation curve showed a relatively sharp unfolding transition with a melting temperature of 42 °C (Fig. 2C) indicating that Art-Est adopted a compact structure. The CD spectrum of Art-Est was strongly dependent on the pH of the solution (Fig. 2D). At pH 3.6, the mean residue ellipticity at 222 nm was −2955 deg cm$^2$ dmol$^{-1}$ residue$^{-1}$, indicating a loss of secondary structure at this pH. However, the secondary structure was relatively stable between pH values of 5 and 8.

The $^1$H-NMR spectrum of Art-Est was assigned from the homonuclear 500 MHz TOCSY and NOESY spectra in 90% $H_2O$ and 10% $D_2O$. All but three backbone NH- and Cα-protons and the majority of the side-chain resonances could be assigned (see ESI†) from both the sequential NH–Cα NOEs and the close similarity to the chemical shift assignment of the residues of bPP. The well resolved region of the amide protons and the large number of cross-peaks in the NOESY spectrum, the majority of which were not observed in the TOCSY spectrum, indicated that Art-Est adopted a well defined, folded structure in solution (see ESI†). The same NOE cross peaks were present in a NOESY experiment at pH 4.1 indicating that the solution structure of Art-Est was stable at lower pH. The large number of NH–NH cross-peaks suggested the presence of significant amounts of α-helical structure. Short- and medium-range NOEs indicated that residues 15–31 were in an α-helical conformation as expected (Chart 1). Over 500 long-range NOEs were observed. NOEs between proline residues in the poly-proline helix and the aromatic and aliphatic residues in the α-helix indicated that the two helices packed together. For instance, NOEs between protons on Hβ, Hγ and Hδ of Pro-2 and protons in the side-chains of Leu-31 and Tyr-27 indicated the close proximity of the C-terminal end of the α-helix and the N-terminal segment of the poly-proline helix. NOEs between Pro-5 and Tyr-20, Leu-24 and Ala-21, as well as between Pro-8 and Tyr-20 and Met-17 indicated that the peptide core was compact. The structure at pH 5.4 was calculated from the magnitude of the NOE cross peaks by standard procedures. Twenty structures were generated in the distance geometry phase of the calculation as a representation of the structure (Fig. 3). Like its parent bPP,[9] Art-Est adopted the classic pancreatic polypeptide fold. The α-helical portion of the peptide appeared folded, ensuring that the catalytic histidine side-chains were constrained in the required conformation. Slight fraying was observed at the N-terminal end of the poly-proline helix. Disordered N-terminal ends of proteins are common and have also been reported for bPP.[9] The fact that the C-terminal end of the α-helix of Art-Est was stably folded enforced the idea that the C-terminal tail of bPP (residues 32–36) is not required for folding or stability. Interestingly, a NOE was observed between the Cα proton of Asn-11 and the amide proton of Leu-31, which was a strong indication that Art-Est formed an anti-parallel dimer in solution under the conditions of the NMR experiments. This had been suggested for bPP based on CD studies and the structure of its close homologue, avian PP (aPP).[16] According to the X-ray structure of aPP,[17] these two residues pack tightly against one another at the heart of the dimer interface.

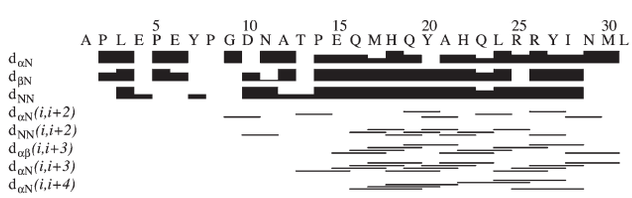


**Chart 1** Amino acid sequence of Art-Est and summary of short-range NOEs involving the NH, CαH and CβH protons. The NOEs are classified as strong, medium and weak as indicated by the thickness of the bar.

### p$K_a$ values of His-18 and His-22

The p$K_a$ values of the two histidines introduced on the solvent exposed face of the α-helix of Art-Est were determined by 1D $^1$H-NMR spectroscopy in $D_2O$. The chemical shifts of the non-labile imidazole protons of His-18 and His-22 were measured over more than eight pH units (pH* 2 to 10.7). By comparison with the spectra at pH 5.4, the histidine resonances could be assigned unequivocally. A titration curve could be assigned to either histidine (Fig. 4) with the corresponding p$K_a$ values of 5.5 and 6.2 for His-22 and His-18, respectively. The p$K_a$ values of the two histidines, which were depressed relative to that of an unperturbed histidine side-chain, were indicative of the success of the design of Art-Est, which was based on destabilising the imidazolium ion of

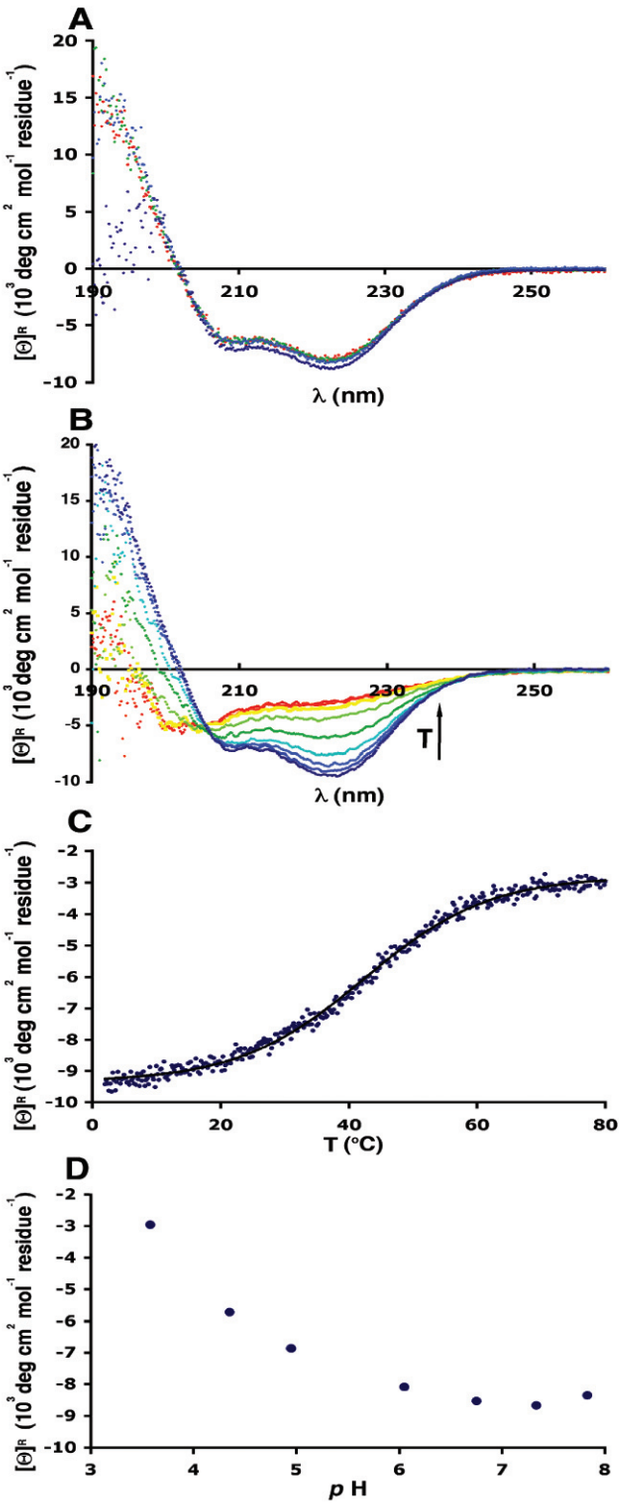


**Fig. 2** Characterisation of the secondary structure of Art-Est by CD spectroscopy. A, CD spectra of 10 μM, 15 μM, 20 μM and 200 μM Art-Est in 5 mM potassium phosphate buffer, pH 7. B, Thermal denaturation of Art-Est (20 μM) between 2 and 82 °C. CD spectra are shown for temperature increments of 10 °C. An arrow indicates the direction of the temperature increase. C, Thermal denaturation of Art-Est depicted as a plot of the mean residue ellipticity $[\Theta]_R$ measured at 222 nm *vs.* the temperature. D, Mean residue ellipticities at 222 nm of a solution of Art-Est (30 μM) *vs.* the pH of the solution.

His-22 through the neighbouring Arg-25 and Arg-26 as well as the stabilisation of His-18 in its protonated form through interaction with the carboxylate group of Glu-15 (Fig. 1B). These results show that significant control and pre-organisation of residues is possible in the solvent exposed environment of the α-helices of Art-Est, maybe supported by neighbouring residues from the second subunit of dimeric Art-Est.

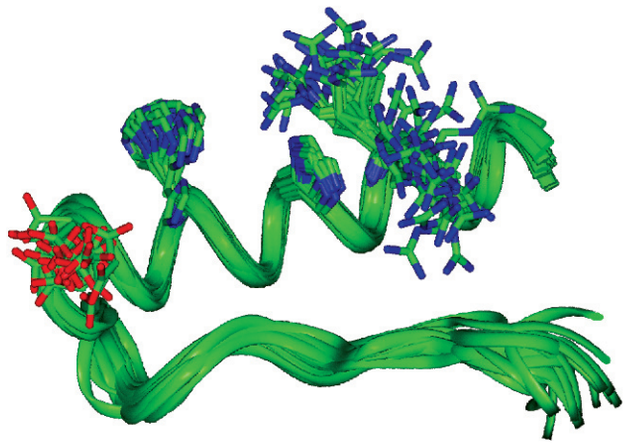

**Fig. 3** Overlay of the atoms of the backbone of Art-Est for 20 structures calculated from the NMR data. The side-chains for the catalytically important residues Glu-15, His-18, His-22, Arg-25 and Arg-26 are also indicated.

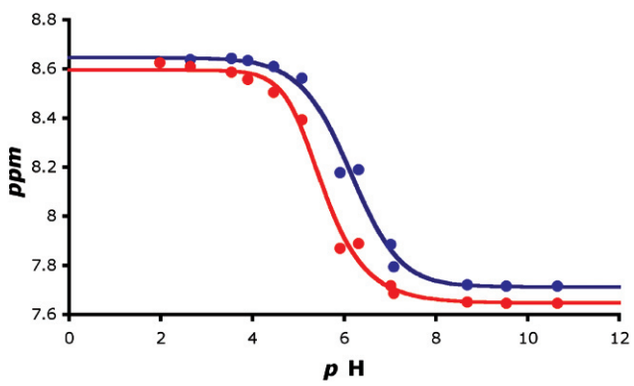


**Fig. 4** pH-titration curves of His-18 (blue) and His-22 (red) of Art-Est (6 mM) measured by NMR spectroscopy at 290 K and the best fit of a function describing the dissociation of a monoprotonic acid.

### Mechanism of the Art-Est catalysed hydrolysis reaction

Art-Est acted as a catalyst for the hydrolysis of *p*-nitrophenyl acetate and mono-*p*-nitrophenyl fumarate (Scheme 1). Ester hydrolysis requires the transfer of an acyl group to a nucleophilic acceptor, which could either be water or an amino acid side-chain of the peptide catalyst. Enzymes that use nucleophilic side-chains normally split the hydrolysis reaction into two steps. In the first, the acyl group is transferred to the nucleophile. Subsequently, hydrolysis of the acyl-enzyme intermediate regenerates the active form of the catalyst. To assess whether a covalent intermediate was observed during catalysis by Art-Est, a five-fold excess of mono-*p*-nitrophenyl fumarate was incubated with Art-Est at pH 5.1. After partial turnover, MALDI-TOF mass spectrometry revealed the presence of small amounts of a peptide whose mass corresponded to Art-Est carrying a single fumaryl group (see ESI†). After complete turnover on the other hand, only free Art-Est was detected by MALDI-TOF mass spectrometry, indicating that the peptide catalysed the hydrolysis of both the *p*-nitrophenyl ester and the acyl-enzyme intermediate.

Further evidence for the Art-Est catalysed conversion of mono-*p*-nitrophenyl fumarate to fumarate by way of an intermediate was obtained by following the time course of the reaction by $^1$H-NMR spectroscopy (Fig. 5). 2.5 mM peptide were incubated with 6.6 mM substrate in $D_2O$ at pH* 6.0 and NMR spectra recorded at regular intervals. The consumption of the substrate was visible in the decrease of the intensity of the signals for its aromatic (8.31 ppm and 7.41 ppm) and olefinic protons (7.05 ppm and 6.68 ppm), while the generation of products could be seen from the increase in the intensity of the signals at 6.49 ppm (fumarate) and 8.11 and 6.92 ppm (*p*-nitrophenol). The rates for the disappearance of the signals for the olefinic and aromatic protons of fumarate were very similar to each other and to the rate of *p*-nitrophenol production (Fig. 6). However, the rate of fumarate production was

substantially slower, in good agreement with the production of a fumaryl-enzyme intermediate. The signal that appeared temporarily in the NMR spectrum around 7.08 ppm after 160 min of reaction may be due to one of the ethylenic protons in the intermediate but the crowding of the NMR spectrum in this region and the relatively low concentration of fumaryl-Art-Est precluded a detailed analysis of the NMR-spectrum of the intermediate.

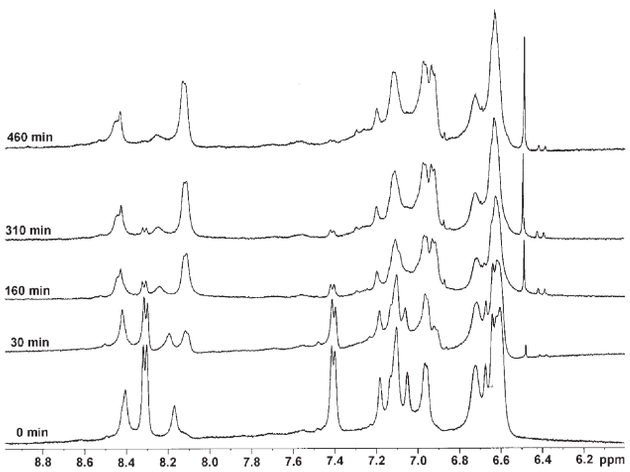


**Fig. 5** NMR time course of the conversion of mono-*p*-nitrophenyl fumarate (6.6 mM) to fumarate and *p*-nitrophenol catalysed by Art-Est (2.5 mM) in $D_2O$ (pH* 6.0). Signals at 8.32, 8.30, 7.42 and 7.40 ppm stem from protons of the *p*-nitrophenyl moiety of the substrate, while the olefinic signals are at 7.05 and 6.68 ppm. Product *p*-nitrophenol signals are at 8.12, 8.11, 6.93, 6.92 ppm; fumarate singlet is at 6.49 ppm.

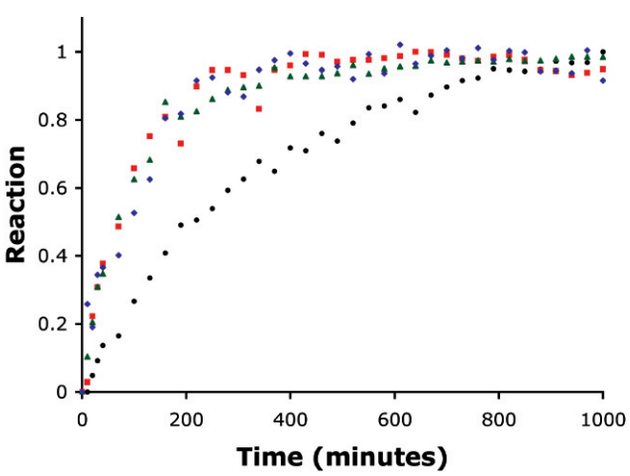


**Fig. 6** Reaction profile of the Art-Est catalysed hydrolysis of mono-*p*-nitrophenyl fumarate monitored by the relative signal integration for individual proton resonances. The graph shows substrate *p*-nitrophenyl doublet around 8.31 ppm (green triangles), fumaryl signal at 7.13 ppm (blue diamonds), product *p*-nitrophenol doublet around 8.11 ppm (red squares) and fumarate (black circles) singlet at 6.49 ppm. Reaction was defined as $I_t/I_{max}$ for product resonances and as $1 - I_t/I_{max}$ for the disappearance of the signals of the substrate, where $I_t$ is the integration at time $t$ and $I_{max}$ the maximal integration.

The hydrolysis of *p*-nitrophenyl esters of acetate and fumarate was followed by UV spectroscopy at 320 nm by monitoring the production of *p*-nitrophenol. Reaction rates were determined under pseudo-first order conditions. The pH dependence of the reaction rates was bell-shaped (Fig. 7).

At pH 4.1, Art-Est enhanced the hydrolysis of mono-*p*-nitrophenyl fumarate by over two orders of magnitude relative to the 4-methyl-imidazole catalysed reactions.[13] The second order rate constant was $9.4 \times 10^{-3}$ $M^{-1}$ $s^{-1}$ (Table 1). The reaction rate increased slightly up to pH values of approximately 5.1 and reached $1.7 \times 10^{-2}$ $M^{-1}$ $s^{-1}$ at that pH value (Table 1). As would be expected for the involvement of nucleophilic catalysis by His-22, the reaction rate for hydrolysis of mono-*p*-nitophenyl fumarate increased sharply around pH 5.5 which corresponds to the p$K_a$

**Table 1** Kinetic parameters for the hydrolysis of *p*-nitrophenyl esters by Art-Est, S-824 and a natural esterase from *E. coli*[a]

| Catalyst | pH | Substrate[b] | $k_2$ (or $k_{cat}/K_M$)/$M^{-1}$ $s^{-1}$ |
|---|---|---|---|
| Art-Est | 4.1 | *p*NPF | $9.4 \times 10^{-3}$ |
| Art-Est | 5.1 | *p*NPF | $1.7 \times 10^{-2}$ |
| Art-Est | 5.1 | *p*NPA | $1.4 \times 10^{-2}$ |
| S-824[23] | 5.1 | *p*NPA | $7.5 \times 10^{-1}$ |
| Art-Est (10% TFE) | 5.1 | *p*NPA | $1.0 \times 10^{-2}$ |
| Art-Est | 6.1 | *p*NPF | $4.8 \times 10^{-2}$ |
| Esterase[24] | 7.1 | *p*NPA | $2.1 \times 10^{4}$ |

[a] Reactions were performed in 100 mM buffer (acetate, pH 5.1; MES, pH 6.1) at 290 K for Art-Est, in 50 mM acetate for S-824 and in 20 mM phosphate for esterase. [b] Substrates used were either mono-*p*-nitrophenyl fumarate (*p*NPF) or acetate (*p*NPA).

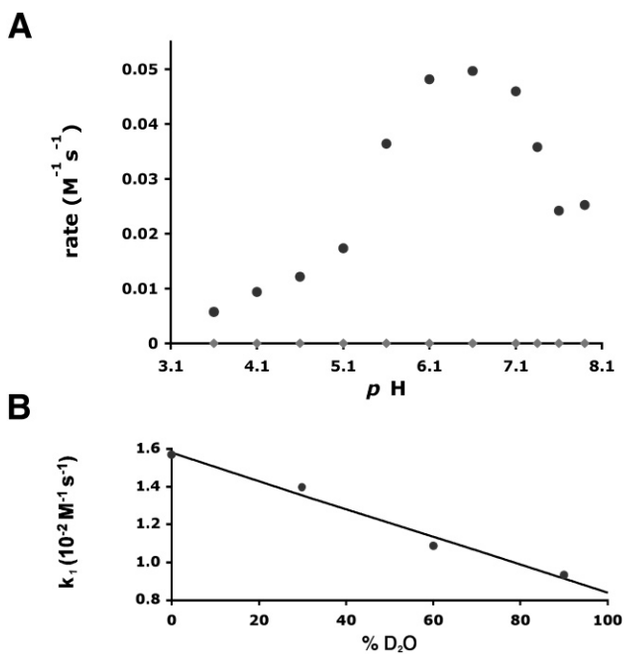


**Fig. 7** A, pH dependence of the rate constants for the spontaneous (♦) (units are in $s^{-1}$) and the Art-Est catalysed (●) hydrolysis of mono-*p*-nitrophenyl fumarate at 290 K; B, proton inventory for the Art-Est (400 μM) catalysed hydrolysis of mono-*p*-nitrophenyl fumarate at pH 5.1 and 290 K.

of His-22. The rate reached a maximum around pH 6.6 where the second order rate constant was $5.0 \times 10^{-2}$ $M^{-1}$ $s^{-1}$. This increase in the reactivity of Art-Est was not due to an increase of the amount of α-helical peptide present since little change in helicity was observed in this range (Fig. 2D). In addition, the presence of 10% of the α-helix-stabilising co-solvent 2,2,2-trifluoroethanol did not lead to an increase in the catalytic rate of the reaction (Table 1). The high reaction rate was maintained up to pH values of approximately 7 (Fig. 7A) followed by a decline of the rate as His-18 became fully deprotonated. This reduction of the activity was not the consequence of a loss of structure of Art-Est since CD spectroscopy indicated that the amount of α-helicity still increased in this pH range (Fig. 2D). More likely, the reduced activity of Art-Est at higher pH values was the consequence of the deprotonation of His-18 resulting in loss of its ability to act as the active-site acid involved in the stabilisation of the transition state preceding the formation of the acyl intermediate between His-22 and the carboxylic acid. The apparent p$K_a$ of 7.35 observed for the decrease of the reaction rate indicated that the p$K_a$ of His-18 was perturbed relative to the value measured for the free catalyst. This may be the consequence of an interaction between $HisH^+$ and the carbonyl oxygen of the substrate or stabilisation of the acyl-anion intermediate (*vide infra*).

To establish whether Arg-25 and Arg-26 not only destabilised the protonated form of His-22 but were also involved in binding the carboxylate group of the substrate mono-*p*-nitrophenyl fumarate, the kinetic experiments were repeated with the uncharged substrate *p*-nitrophenyl acetate. At pH 5.1, the second order rate constant for

the Art-Est catalysed hydrolysis of mono-*p*-nitrophenyl fumarate ($k_2 = 1.7 \times 10^{-2}$ $M^{-1}$ $s^{-1}$) was only slightly higher than that of the hydrolysis of *p*-nitrophenyl acetate ($k_2 = 1.4 \times 10^{-2}$ $M^{-1}$ $s^{-1}$) (Table 1) indicating that Art-Est showed only a slight preference for anionic substrates. The pH rate profile for the hydrolysis of mono-*p*-nitrophenyl fumarate indicated that the reactive species of the peptide had the mainly unprotonated imidazole of His-22 flanked by the more basic, mainly protonated His-18, in good agreement with the design of Art-Est (Fig. 1).

Solvent kinetic isotope effects are good probes of the mechanism of a reaction. The proton inventory determined at pH* 5.1 revealed a linear dependence of the second order rate constant for the Art-Est catalysed hydrolysis of mono-*p*-nitrophenyl fumarate on the percentage of $D_2O$ in the reaction (Fig. 7B). From this proton inventory, a solvent kinetic isotope effect of 1.8 could be determined. A solvent kinetic isotope effect of this magnitude is generally interpreted as an indication of strong hydrogen bonding in the transition state and/or general acid base catalysis. The solvent KIE observed here, which was similar to the values typically observed for natural esterases,[18] suggested that Art-Est stabilised the transition state preceding the acyl intermediate through the protonated side-chain of His-18.

In conclusion, Art-Est catalysed the efficient hydrolysis of *p*-nitrophenyl esters as a result of its stable, well-defined three-dimensional solution structure. The pancreatic polypeptide fold appears to provide a versatile scaffold for the production of miniature enzymes with various activities. Art-Est followed a mechanism similar to that observed for natural esterases with active sites deeply buried within their structure, albeit with reduced catalytic activity.[18] The active site of Art-Est was based on two histidines with perturbed p$K_a$ values due to their proximity to one another and to neighbouring residues such as Glu-15, Arg-25 and Arg-26. This active site configuration led to a bell-shaped pH dependence of the catalytic rates. While reports of designed peptides with esterase activities have been published previously, the bell-shaped pH dependence of the activity that would be expected from the interplay of two catalytic histidines has never before been observed in rationally designed peptides.[13,19,20] A bell-shaped catalytic profile was obtained for a 102-residue protein, S-824, that was selected from a large 2nd generation library of binary patterned proteins.[21–23] Despite being the result of selection from a large pool of proteins, the catalytic activity of S-824 was only 50 times higher than that observed for Art-Est and it is unclear whether the apparent p$K_a$ values corresponded to a change in the protonation state of the catalytic histidines of S-824 (Table 1). The catalytic behaviour of Art-Est therefore indicated that even in the absence of an active site pocket shielded from the solvent, designed miniature enzymes can act in a transparent mechanism based fashion with enzyme-like behaviour through the interplay of several amino acid residues.

## Acknowledgement

The help of Neil Spencer, Peter R. Ashton and Graham Burns with NMR, mass spectrometry and chromatography is gratefully acknowledged. The authors would like to acknowledge financial support from the BBSRC, EPSRC and the University of Birmingham and stimulating discussions with Chris Weston and Oliver Smart.

## References

1 M. K. H. Pflum, *Chem. Biol.*, 2004, **11**, 3.
2 J. K. Montclare and A. Schepartz, *J. Am. Chem. Soc.*, 2003, **125**, 3416.
3 J. W. Chin and A. Schepartz, *J. Am. Chem. Soc.*, 2001, **123**, 2929.
4 N. J. Zondlo and A. Schepartz, *J. Am. Chem. Soc.*, 1999, **121**, 6938.
5 E. C. Turner, C. H. Cureton, C. J. Weston, O. S. Smart and R. K. Allemann, *Chem. Biol.*, 2004, **11**, 69.
6 S. E. Taylor, T. J. Rutherford and R. K. Allemann, *Bioorg. Med. Chem. Lett.*, 2001, **11**, 2631.
7 S. E. Taylor, T. J. Rutherford and R. K. Allemann, *J. Chem. Soc., Perkin Trans. 2*, 2002, 751.
8 K. Johnsson, R. K. Allemann, H. Widmer and S. A. Benner, *Nature*, 1993, **365**, 530.
9 X. Li, M. J. Sutcliffe, T. W. Schwartz and C. M. Dobson, *Biochemistry*, 1992, **31**, 1245.
10 L. Baltzer, A. C. Lundh, K. Broo, S. Olofsson and P. Ahlberg, *J. Chem. Soc., Perkin Trans. 2*, 1996, 1671.
11 K. Wüthrich, *NMR of proteins and nucleic acids*, John Wiley & Sons, New York, 1986.
12 A. T. Brunger, P. D. Adams, G. M. Clore, W. L. DeLano, P. Gros, R. W. Grosse-Kunstleve, J. S. Jiang, J. Kuszewski, M. Nilges, N. S. Pannu, R. J. Read, L. M. Rice, T. Simonson and G. L. Warren, *Acta Crystallogr. Sect. D—Biol. Crystallogr.*, 1998, **54**, 905.
13 K. S. Broo, L. Brive, P. Ahlberg and L. Baltzer, *J. Am. Chem. Soc.*, 1997, **119**, 11362.
14 P. J. Chang, M. E. Noelken and J. R. Kimmel, *Biochemistry*, 1980, **19**, 1844.
15 M. E. Noelken, P. J. Chang and J. R. Kimmel, *Biochemistry*, 1980, **19**, 1838.
16 I. D. Glover, D. J. Barlow, J. E. Pitts, S. P. Wood, I. J. Tickle, T. L. Blundell, K. Tatemoto, J. R. Kimmel, A. Wollmer, W. Strassburger and Y. S. Zhang, *Eur. J. Biochem.*, 1984, **142**, 379.
17 T. L. Blundell, J. E. Pitts, I. J. Tickle, S. P. Wood and C. W. Wu, *Proc. Natl. Acad. Sci. USA*, 1981, **78**, 4175.
18 L. D. Sutton, J. S. Stout and D. M. Quinn, *J. Am. Chem. Soc.*, 1990, **112**, 8398.
19 K. S. Broo, H. Nilsson, J. Nilsson, A. Flodberg and L. Baltzer, *J. Am. Chem. Soc.*, 1998, **120**, 4063.
20 L. Baltzer and J. Nilsson, *Curr. Opin. Biotechnol.*, 2001, **12**, 355.
21 Y. N. Wei, S. Kim, D. Fela, J. Baum and M. H. Hecht, *Proc. Natl. Acad. Sci. USA*, 2003, **100**, 13270.
22 Y. N. Wei, T. Liu, S. L. Sazinsky, D. A. Moffet, I. Pelczer and M. H. Hecht, *Protein Sci.*, 2003, **12**, 92.
23 Y. Wei and M. H. Hecht, *Protein Eng. Des. Select.*, 2004, **17**, 67.
24 S. Kanaya, T. Koyanagi and E. Kanaya, *Biochem. J.*, 1998, **332**, 75.